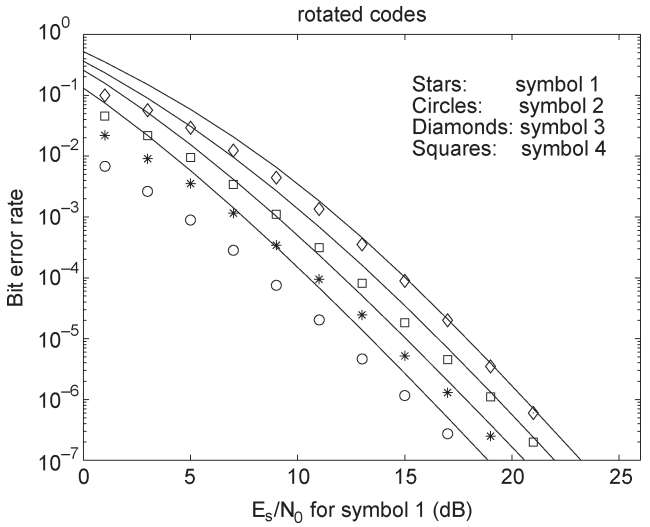

Fig. 3. (Markers) Simulation and (solid lines) analytic BERs for the GO-MC-CDM system with four subcarriers per group (full load) using rotated W–H codes (right).

expression is able to predict phenomena such as the loss of diversity experienced by symbol 1 when using nonrotated codes. Interestingly, this diversity loss when using W–H codes is fairly moderate when compared with the situation where all symbols in the group employ equal modulation [6] and are received with equal power (e.g., strict power control is in operation); in the latter case, downlink W–H spreading results in a very poor BER performance.

V. Conclusion

This paper has presented a new analytical BER expression for GO-MC systems using ML detection. The derived expression, which is suitable for either uplink or downlink scenarios, generalizes previous expressions by allowing the different symbols forming a group to come from different modulation alphabets and to have different received powers. Both features are likely to occur in situations where users have distinct QoS requirements and/or when no power control mechanism is in operation. Simulation results using typical parameters currently found in WLANs show a good agreement with the derived BER upper bound for the usually relevant BER range, suggesting that this analytical expression is a valuable tool for the planning of GO-MC systems.

References

[1] X. Cai, S. Zhou, and G. Giannakis, "Group-orthogonal multicarrier CDMA," *IEEE Trans. Commun.*, vol. 52, no. 1, pp. 90–99, Jan. 2004.

[2] N. Yee, J.-P. Linnartz, and G. Fettweis, "Multi-carrier CDMA in indoor wireless radio networks," in *Proc. IEEE Int. Symp. Pers., Indoor, Mobile Radio Commun.*, Yokohama, Japan, Sep. 1993, pp. 109–113.

[3] F. Riera-Palou, G. Femenias, and J. Ramis, "On the design of group orthogonal MC-CDMA systems," in *Proc. IEEE Signal Process. Advances Wireless Commun.*, Cannes, France, Jul. 2006, pp. 1–5.

[4] F. Riera-Palou, G. Femenias, and J. Ramis, "On the design of uplink and downlink group-orthogonal multicarrier wireless systems," *IEEE Trans. Commun.*, vol. 56, no. 9, Oct. 2008.

[5] S. Kaiser, "OFDM code-division multiplexing in fading channels," *IEEE Trans. Commun.*, vol. 50, no. 8, pp. 1266–1273, Aug. 2002.

[6] F. Riera-Palou, G. Femenias, and J. Ramis, "Performance of downlink group-orthogonal multicarrier systems," in *Proc. IFIP Pers. Wireless Commun.*, Albacete, Spain, Sep. 2006, pp. 389–400.

[7] J. Proakis, *Digital Communications*, 3rd ed. New York: McGraw-Hill, 1996.

[8] D. Divsalar and M. Simon, "Multiple-symbol differential detection of MPSK," *IEEE Trans. Commun.*, vol. 38, no. 3, pp. 300–308, Mar. 1990.

[9] M. Simon, S. Hinedi, and W. Lindsey, *Digital Communication Techniques—Signal Design and Detection*. Englewood Cliffs, NJ: Prentice-Hall, 1994.

[10] J. W. Craig, "A new, simple and exact result for calculating the probability of error for two-dimensional signal constellations," in *Proc. IEEE MILCOM Conf. Rec.*, Boston, MA, 1991, pp. 571–575.

[11] M. K. Simon and M.-S. Alouini, *Digital Communication Over Fading Channels*, 2nd ed. Chichester, U.K.: Wiley, 2005.

[12] G. Femenias, "BER performance of linear STBC from orthogonal designs over MIMO correlated Nakagami-m fading channels," *IEEE Trans. Veh. Technol.*, vol. 53, no. 2, pp. 307–317, Mar. 2004.

[13] S. V. Amari and R. B. Misra, "Closed-form expressions for distribution of sum of exponential random variables," *IEEE Trans. Rel.*, vol. 46, no. 4, pp. 519–522, Dec. 1997.

[14] J. Medbo and P. Schramm, "Channel models for HIPERLAN/2 in different indoor scenarios," ETSI, Sophia Antipolis, Nice, ETSI-BRAN, Tech. Rep. 3ERI085B, Mar. 1998.

[15] A. Doufexi, S. Armour, M. Butler, A. Nix, D. Bull, J. McGeehan, and P. Karlsson, "A comparison of the HIPERLAN/2 and IEEE 802.11a wireless LAN standards," *IEEE Commun. Mag.*, vol. 40, no. 5, pp. 172–180, May 2002.

[16] A. Bury, J. Egle, and J. Lindner, "Diversity comparison of spreading transforms for multicarrier spread spectrum transmission," *IEEE Trans. Commun.*, vol. 51, no. 5, pp. 774–781, May 2003.

Bit-Interleaved Sphere-Packing-Aided Iteratively Detected Space-Time Coded Modulation

Ronald Y. S. Tee, Osamah Alamri, Soon Xin Ng, and Lajos Hanzo

***Abstract*—We design a bit-interleaved space-time coded modulation scheme using iterative decoding (BI-STCM-ID) combined with a new multidimensional mapping scheme invoking sphere-packing (SP) modulation, which we refer to as the space-time block-coded sphere-packed bit-interleaved coded modulation (STBC-SP-BICM) arrangement. The binary switching algorithm (BSA) is used to optimize the cost function employed for deriving different mapping strategies, which are designed with the aid of EXtrinsic Information Transfer (EXIT) charts for the sake of improving the convergence behavior of the system. The resultant system is amalgamated with a unity-rate code (URC) as a precoder to enhance the attainable iterative detection performance. An irregular URC (IrURC) is invoked to create an open EXIT tunnel at low signal-to-noise ratios (SNRs). The complexity of employing the multidimensional SP scheme is also addressed.**

***Index Terms*—Bit-interleaved space-time coded modulation, extrinsic information transfer (EXIT) charts, iterative detection, set partitioning, sphere-packing modulation, unity-rate coding.**

I. Introduction

Alamouti's space-time block codes (STBCs) [1] constitute an elegant way of implementing a simple twin-antenna design for providing second-order diversity at the transmitter, which was further generalized to an arbitrary number of transmitters by Tarokh *et al.* [2]. However, no attempt was made to jointly design the multiple antennas' signals; hence, this joint design is addressed in this paper with the aid of sphere-packing (SP) modulation [3].

Manuscript received May 22, 2007; revised April 14, 2008 and April 25, 2008. First published May 14, 2008; current version published January 16, 2009. The review of this paper was coordinated by Prof. N. Arumugam.

The authors are with the University of Southampton, S017 1BJ Southampton, U.K.

Digital Object Identifier 10.1109/TVT.2008.925299

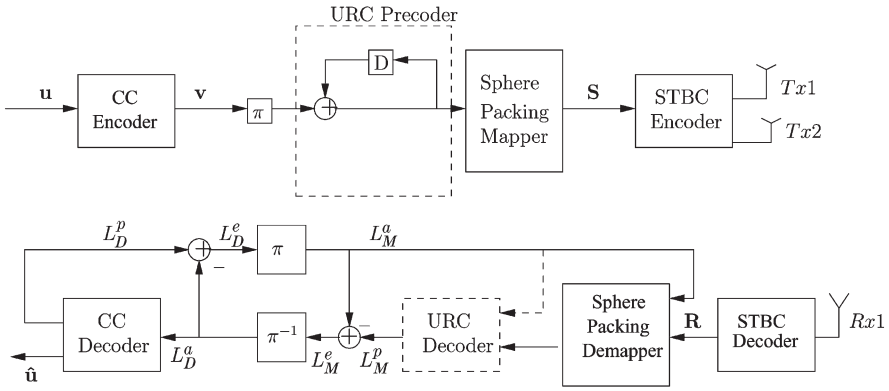

Fig. 1. STBC-SP-BICM scheme.

Bit-interleaved coded modulation (BICM) was designed by Zehavi [4] as a joint coding and modulation scheme for increasing the Hamming distance of the code for transmission over fading channels. Independent bit interleavers were used in conjunction with Gray mapping of the bits to constellation points for increasing the achievable time-diversity order and, consequently, enhancing the effective code length. An iterative BICM detector was introduced by Li and Ritcey [5] by employing Ungerböck partitioning (UP)-based bit mapping to improve the minimum Euclidean distance and achieve an iteration gain, compared to that of a noniterative BICM. The BICM-ID UP-based mapping scheme was further improved in [6] and [7].

As further enhancement of the aforementioned schemes, bit-interleaved space-time coded modulation using iterative decoding (BI-STCM-ID) was introduced by combining BICM with STBC while employing separate bit interleavers [8]–[10], where the specific choice of constellation labeling determines the BICM-ID scheme's performance. A novel SP scheme combined with orthogonal transmit diversity design [11] was introduced by Su *et al.* [12], which was further developed by Alamri *et al.* [3] using an SP- and turbo-detection-aided concatenated STBC design [12].

Motivated by these substantial performance improvements, in this treatise, we further develop the SP concept using a BICM scheme to create an improved orthogonal transmit diversity design, where the harmonic mean Euclidean distance of space-time symbols defined in an M-dimensional (M-D) space is maximized by finding the most meritorious mapping of the bits to the signaling constellation.

Hence, the novelty of this paper is that we propose a new space-time block-coded sphere-packed bit-interleaved coded modulation (STBC-SP-BICM) arrangement. In contrast to Alamouti's scheme, we jointly design the space-time signal of the two space-time slots. We investigate its performance in conjunction with various bit-to-SP-symbol mapping strategies compared with the identical-throughput conventional quadrature phase-shift keying (QPSK) and 16-state quadrature amplitude modulation (16QAM) schemes. Furthermore, a unity-rate code (URC) [13] is amalgamated with the SP mapper to improve the attainable iterative gain. EXtrinsic Information Transfer (EXIT) chart analysis is employed to investigate the convergence behavior of the proposed system. An irregular URC (IrURC) is proposed to create an open EXIT tunnel at low SNRs. We adopt the Euclidean distance between the different SP constellation points as our cost function (CF), which is minimized using the binary switching algorithm (BSA) [7]. The constellation points of the four-dimensional (4-D) SP scheme are categorized into different SP layers according to their Euclidean distance from the origin [12], and the bit-to-SP-symbol mapping is optimized by the BSA using our CF.

This paper is organized as follows: In Section II, an overview of our proposed STBC-SP-BICM scheme is presented, whereas the various mapping schemes and their complexity are characterized in Section III. These discussions are followed by our EXIT chart analysis in Section IV and by the IrURC structure in Section V. Our simulation results are presented in Section VI. Finally, we conclude our discourse in Section VII.

II. System Overview

Fig. 1 shows the schematic of the proposed STBC-SP-BICM arrangement, where a convolutional code (CC) is used as the outer code. Binary source bit stream $\mathbf{u}$ is encoded by the CC, and the encoded bit stream denoted by $\mathbf{v}$ is then bit interleaved by the block π in Fig. 1. The SP symbol set $\mathbf{S}$ is fed to the STBC encoder having two transmitter antennas.

At the receiver, the received SP symbol set $\mathbf{R}$ is fed into the SP demapper by the STBC decoder. The *a posteriori* log-likelihood ratios (LLRs) L_M^p at the output of the SP demapper shown in Fig. 1 are subtracted from the *a priori* LLRs L_M^a to obtain the *extrinsic* LLRs L_M^e. This *extrinsic* information is then deinterleaved and fed—as the *a priori* LLR L_D^a—to the CC decoder in Fig. 1. When using iterative decoding, the *a posteriori* coded LLRs L_D^p generated by the CC decoder are used for obtaining the *extrinsic* LLR L_D^e by subtracting the corresponding *a priori* LLR L_D^a in Fig. 1. Again, the useful *extrinsic* information is fed through the bit interleaver π and serves as the *a priori* LLR L_M^a input of the SP demapper. The SP mapper assigns the bits to different SP constellation points using various bit-to-SP-symbol mapping schemes, as outlined later in Section III.

To reach the point of iterative convergence, additionally, a URC's encoder [13] is introduced as a precoder, as shown in the box plotted in dashed line in Fig. 1. When the URC precoder is introduced, L_M^p becomes the *a posteriori* LLR of the URC decoder instead of the SP demapper. Hence, the *extrinsic* LLR L_D^e in Fig. 1 is fed as the *a priori* coded LLR into the URC's decoder. The decoding iterations will then be continued by exchanging *extrinsic* information between the CC decoder and the URC decoder, as shown by the dashed arrow in Fig. 1.

To further elaborate on the design of the soft SP demapper, we first consider the 4-D SP phasor points, which are denoted as $S = (a_{l,1}, a_{l,2}, a_{l,3}, a_{l,4})$, where we have $l = 0, 1, 2, \ldots, M-1$ and M is the number of SP constellation points. Here, we would like to represent the four individual coordinates of S in the 4-D SP space representing the space-time slots using real values while satisfying the D_4 SP constraint[1] of $(a_1 + a_2 + a_3 + a_4) = k$, where k is an even

[1] D_4 is a 4-D lattice having the best Euclidean distance in the 4-D real Euclidean space $\mathbb{R}^4$ [14].

integer constant [14]. The total energy of the signal points is represented by $E \triangleq \sum_{l=0}^{M-1}(|a_{l,1}|^2 + |a_{l,2}|^2 + |a_{l,3}|^2 + |a_{l,4}|^2)$ [12].

The joint space-time symbol design of the two antennas entails that, after SP modulation, the 4-D SP symbol is mapped to two complex-valued 2-bit symbols of a twin-antenna STBC scheme. The bit-to-SP-symbol mapping function of the system is denoted as [3] $\Gamma(\psi(b^1, b^2, b^3, b^4)) = \{a_{l,1} + ja_{l,2}, a_{l,3} + ja_{l,4}\} = \{x_{l,1}, x_{l,2}\}$, where $\psi(.)$ is the SP function used for mapping the original input bits to the SP symbols and $\Gamma(.)$ represents the mapping of the 4-D SP symbols to the complex-valued 2-bit symbols $x_{l,1}$ and $x_{l,2}$ after STBC encoding.

The *extrinsic* LLR of a single bit b_k output by the demodulator can be expressed as [3]

$$\begin{aligned} & L(b_k|\mathbf{R}) - L_a(b_k) \\ & = \ln \frac{\sum_{\mathbf{S}^l \in S_1^k} \exp\left[-\frac{(\mathbf{R}-\alpha\cdot\mathbf{S}^l)(\mathbf{R}-\alpha\cdot\mathbf{S}^l)^T}{2\sigma_w^2} + \sum_{j=0,j\neq k}^{B-1} b_j L_a(b_j)\right]}{\sum_{\mathbf{S}^l \in S_0^k} \exp\left[-\frac{(\mathbf{R}-\alpha\cdot\mathbf{S}^l)(\mathbf{R}-\alpha\cdot\mathbf{S}^l)^T}{2\sigma_w^2} + \sum_{j=0,j\neq k}^{B-1} b_j L_a(b_j)\right]} \\ & = \max_{\mathbf{S}^l \in S_1^k}\left[-\frac{1}{2\sigma_w^2}(\mathbf{R}-\alpha\cdot\mathbf{S}^l)(\mathbf{R}-\alpha\cdot\mathbf{S}^l)^T + \sum_{j=0,j\neq k}^{B-1} b_j L_a(b_j)\right] \\ & \quad - \max_{\mathbf{S}^l \in S_0^k}\left[-\frac{1}{2\sigma_w^2}(\mathbf{R}-\alpha\cdot\mathbf{S}^l)(\mathbf{R}-\alpha\cdot\mathbf{S}^l)^T + \sum_{j=0,j\neq k}^{B-1} b_j L_a(b_j)\right] \end{aligned} \tag{1}$$

where the SP symbols carry B number of bits $\mathbf{b} = b_0, \ldots, b_{B-1} \in \{0, 1\}$. Let us furthermore assume that S_1^k and S_0^k represent two specific 2-D subsets of the 4-D SP symbol constellation S, which obey $S_1^k \triangleq \{\mathbf{S}^l \in S : b_k = 1\}$ and $S_0^k \triangleq \{\mathbf{S}^l \in S : b_k = 0\}$, respectively. The max-log approximation is used to simplify the equation for low-complexity implementation, as described in Section III-C.

III. Mapping Scheme

Again, the legitimate constellation points hosted by D_4 are organized into layers based on their norms or energy, i.e., the distance from the origin. We investigate the first ten layers of the D_4 SP constellation points [14]. For example, the SP symbol centered at $\{0, 0, 0, 0\}$ has 24 closest neighbor SP symbols around it since any combination of $\{+/-1, +/-1, 0, 0\}$ is legitimate for layer 1 [14], which are listed in rows 0–15 of Table I.

Two different STBC-SP-BICM schemes having constellation sizes of $M = 16$ and $M = 256$ are investigated, which are referred to as SP-16 and SP-256, respectively. First, for a 4-D SP-16 symbol, the throughput of the STBC-SP arrangement τ using no outer CC encoder is $\tau = 1$ symbol/(2 time slot) $\times$ 4 b/symbol $= 2$ b/(time slots) $=$ 2 b/(channel use). Hence, uncoded QPSK is the corresponding equivalent conventional modulation having the same throughput of $\tau = 2$ symbol/(2 time slot) $\times$ 2 b/symbol $= 2$ b/(channel use). Since there are 24 immediately adjacent neighbors at layer 1 having different Euclidean distances from the $\{0, 0, 0, 0\}$ symbol in the 4-D SP constellation [14], we select the particular 16 points that exhibit maximum Euclidean distances.

First, the SP signal constellation points D_4 having the maximum Euclidean distance between adjacent or nearest neighbor points at a given energy level found by an exhaustive search are used. The first set of labeling based on this constellation space is obtained by an exhaustive computer search for maintaining the maximum Euclidean distance between the complementary bits of a specific partitioned sphere-packing constellation point set (as in classic set partitioning),

TABLE I
BIT MAPPINGS FOR DIFFERENT SCHEMES FOR STBC-SP USING $M = 16$

Index	L-1 and L-2 Points D_4				Symbol Index, $S_i = j, i \in \{0...15\}$			
j	a_1	a_2	a_3	a_4	Gray	SET	L1-BSA	L2-BSA
0	−1	−1	0	0	0	1	0	3
1	0	−1	−1	0	1	0	5	12
2	0	−1	+1	0	2	8	2	5
3	+1	−1	0	0	3	9	15	0
4	−1	0	0	+1	4	2	13	15
5	0	0	−1	+1	5	7	6	9
6	0	0	+1	+1	6	4	14	10
7	+1	0	0	+1	7	5	10	6
8	−1	0	0	−1	8	2	12	16
9	0	0	−1	−1	9	15	11	17
10	0	0	+1	−1	10	7	4	18
11	+1	0	0	−1	11	6	1	19
12	−1	+1	0	0	12	13	3	20
13	0	+1	−1	0	13	3	8	21
14	0	+1	+1	0	14	11	9	22
15	+1	+1	0	0	15	10	7	23
16	-2	0	0	0	-	-	-	-
17	0	0	-2	0	-	-	-	-
18	2	0	0	0	-	-	-	-
19	0	2	0	0	-	-	-	-
20	0	-2	0	0	-	-	-	-
21	0	0	2	0	-	-	-	-
22	0	0	0	2	-	-	-	-
23	0	0	0	-2	-	-	-	-

as shown in Table I. The BSA [7] is then employed for generating different SP mapping schemes. First, we propose a specific mapping CF, which quantifies the reciprocal of the squared Euclidean distance of each SP symbol with respect to other SP symbols within a specific partitioned subset. The CF can be formulated as

$$CF = \sum_{i=0}^{m-1} \sum_{b=0}^{1} \sum_{S_k \in \Gamma_b^i} \frac{1}{|S_k - \hat{S}_k|^2}. \tag{2}$$

We assume here that the SP demapper has perfect *a priori* information and that the SP signal space has $M = 2^m$ constellation points. The notation Γ represents the SP-to-STBC symbol mapping function, namely, that converting bits $b \in \{0, 1\}$ to symbols S_k. Symbol $\hat{S}_k$ is the nearest neighbor of S_k in the 4-D SP space, which is mapped according to $\Gamma_{\overline{b}}^i$, where $\overline{b}$ denotes the complement of bit b at bit index i.

By minimizing the CF of (2) using the BSA, a special partitioning is obtained, corresponding to maximizing the harmonic means of the Euclidean distances of the SP constellation points belonging to the opposite bit values at the same partitioning level in the whole mapping scheme. In other words, we search for the specific SP symbol S_k, where the counterpart symbol $\hat{S}_k$ $(k = 0, \ldots, 2^m - 1)$ having the same binary bit label, except for the ith bit, has the maximum total summed Euclidean distance for all symbol pairs within the particular set considered.

A. SP-16 Constellation Points

We call this a layer-1 BSA (L1-BSA)-aided mapping, and the resultant symbol indexes are given in Table I. We then further extend the constellation by introducing the layer-2 constellation points in the space to explore a larger variety of SP constellations while maintaining a fixed total power. There are a total of 24 points in layer 2 [14]. For example, here, we opt to select the eight highest distances from layer 1 and the eight highest distance points from layer 2 to form a new constellation. By using (2), we obtain a different bit-to-SP mapping scheme for this constellation, and we call this the BSA layer-2-aided (L2-BSA) scheme, which is shown in Table I.

The index shown in the first column of Table I outlines the selected constellation points for both layers 1 and 2 after finding the points that have the maximum Euclidean distance in the D_4 search space. Note that the layer-1 points span from index $i = 0$ to 15, indicating the 16 points of layer 1, and that the layer-2 points span from index $i = 16$ to 23. The notation $S_i = j$ indicates that SP symbol S_i is assigned to the constellation points of each index j, as tabulated. The index i associated with symbol S_i is in increasing order from "0" to "15." For example, referring to the L1-BSA mapping scheme in Table I, the first three rows are 0, 5, and 2, which indicate the SP symbols of S_0, S_1, and S_2. These symbols are associated with the indexes of 0, 5, and 2, which correspond to the constellation points of $\{-1, -1, 0, 0\}$, $\{0, 0, -1, +1\}$, and $\{0, -1 + 1, 0\}$, respectively.

B. SP-256 Constellation Points

For a 4-D SP symbol having a total constellation size of $M = 256$ (SP-256), the throughput of the STBC-SP arrangement τ operating without an outer CC encoder is $\tau = 1$ symbol/(2 time slot) $\times$ 8 b/symbol $= 4$ b/(time slot) $= 4$ b/(channel use). The throughput of this STBC-SP SP-256 scheme corresponds to that of a classic 16QAM STBC scheme.

We further investigate this SP-256 scheme by selecting 256 constellation points from a single layer of the SP signal space, which is constituted by M constellation points, where we have $M \geq 256$. The layer-9 SP D_4 space has a total of $N = 312 \geq 256$ constellation points [14] and, hence, satisfies our selection constraint. Then, upon applying the BSA for optimizing the CF of (2), we arrive at the optimized mapping, which we call the L9-BSA scheme. As an alternative second approach, let us now select the SP constellation points from different layers of the D_4 SP space, ranging from layers 1 to 5. This scheme has a total of 312 constellation points [14]. Employing the CF of (2) again, we generate the bit-to-SP mapping scheme having the minimum CF by applying the BSA. The second mapping scheme is called the BSA-multilayer arrangement.

For the sake of convenience, we summarize the various schemes in Table II. Observe in Table II that we refer to the systems using SP-16-aided mapping schemes as System 1 and System 2, whereas we refer to the systems using SP-256-aided mapping schemes as System 3 and System 4.

C. Complexity Issues

The SP-16 and SP-256 constellation schemes impose a different implementational complexity. The M-D SP constellation outperforms classic 16QAM having the same overall system throughput in the STBC-SP-BICM scheme, at the cost of higher complexity, as addressed here for comparison. From (1), we can determine the number of Add, Compare, and Select (ACS) arithmetic operations, when these operations are carried out in the logarithmic domain while using a lookup table to implement the Jacobian approximation used in the max-log-MAP algorithm. The terms $O_{\text{ACS}}^{\text{SP}-16}$ and $O_{\text{ACS}}^{\text{SP}-256}$ denote the ACS operations per source bit imposed by the log-MAP decoder of the SP-16 and SP-256 schemes, respectively.

From these computations, we infer the number of ACS operations given by $O_{\text{ACS}}^{\text{SP}-16} = 130.18$ and $O_{\text{ACS}}^{\text{SP}-256} = 2850.72$ for our novel SP mapper. Note that the classic 16QAM scheme having the same throughput as SP-256 would exhibit a similar ACS complexity, i.e., $O_{\text{ACS}}^{16QAM} = 130.18$, when employing the max-log-MAP algorithm. Therefore, the cost of achieving the improved performance shown in Fig. 5 would impose an ACS complexity that is approximately 20 times higher than a classic 16QAM scheme.

TABLE II
SYSTEM PARAMETERS

Sphere packing modulation	$M = 16$, $M = 256$
Conventional modulation	QPSK, 16QAM
STBC-SP-BICM output block length	2560 bits
Channel	Correlated Rayleigh Fading
Normalised Doppler frequency	0.1
Outer CC	(2,1,5)
Generator Polynomial for CC memory-4 memory-1	 $(G_1, G_2) = (23_8, 25_8)$ $(1, G_1/G_2) = (1, 2_8/1_8)$
Generator Polynomial for URC precoder	$G(D) = 1/(1 + D)$
Throughput STBC-SP $M = 16$ STBC-QPSK	 (without outer code) 2 bits/channel use
Throughput STBC-SP, $M = 256$ STBC-16QAM	 (without outer code) 4 bits/channel use
System Without Precoder System-1 System-2 System-3 System-4	 SP-16, Gray SP-16, SET SP-256, L9-BSA SP-256, BSA-Multilayer
System With Precoder System-5 System-6 System-7	 SP-16, Gray SP-16, L1-BSA SP-16, L2-BSA

IV. STBC-SP-BICM WITH EXIT CHART ANALYSIS

The concept of EXIT charts was proposed in [15] for the semianalytic investigation of the convergence of iterative decoders, where the exchange of mutual information between two component codes is visualized. In our STBC-SP-BICM scheme, the output of the outer CC code is interleaved for providing an independent source of extrinsic information for the iterative receiver. Typical EXIT curves are generated under the assumptions that a high interleaver length is used and that the probability density function of the *a priori* LLRs is Gaussian distributed.

The *a priori* LLR information L_D^a of the outer CC code of Fig. 1 can be modeled by an independent zero-mean Gaussian random variable. The EXIT characteristic of the outer CC decoder is independent of the channel's E_b/N_0 value and, hence, can be formulated as $I_{E,CC} = T_{\text{CC}}(I_{A,CC})$, where $I_{A,CC} = I(V; L_D^a)$ is the mutual information between the outer CC's encoded bits V and the LLR value L_D^a.

As for the inner SP demapper operating without a precoder, the *a priori* LLRs L_M^a can be modeled by a Gaussian distribution, and the corresponding mutual information $I_{A,SP} = I(V; L_M^a)$ is a function of V and L_M^a. By contrast, the demapper's EXIT characteristic depends on E_b/N_0 and hence can be formulated as $I_{E,SP} = T_{\text{SP}}(I_{A,SP}, E_b/N_0)$. Following the introduction of the URC precoder, the *a priori* information L_M^a is generated at the input of the URC decoder, as shown by the arrow drawn in dashed line in Fig. 1. The corresponding modified EXIT characteristic $I_{E,SP}$ must be computed with the aid of L_M^e gleaned from the URC decoder's output. The precoded mapping schemes are summarized in Table II as System 5–System 7.

V. IrURC STRUCTURE

Based on the EXIT chart analysis in Fig. 2, we further improved our precoded STBC-SP-BICM scheme with the aid of an IrURC precoder structure to create an EXIT tunnel at a reduced SNR. With the aid of the IrURC, we may use a weaker CC to achieve a given bit error

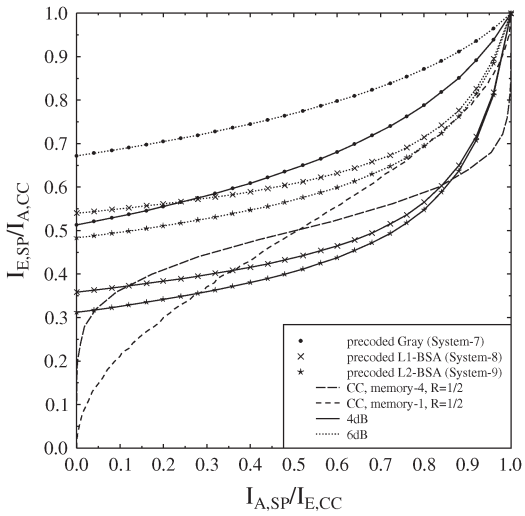

Fig. 2. Comparison of the convergence behavior of the precoded systems using the STBC-SP-BICM demapper employing a URC precoder. The EXIT charts shown are based on the parameters outlined in Table II when operating at both $E_b/N_0 = 4$ dB and 6 dB, respectively.

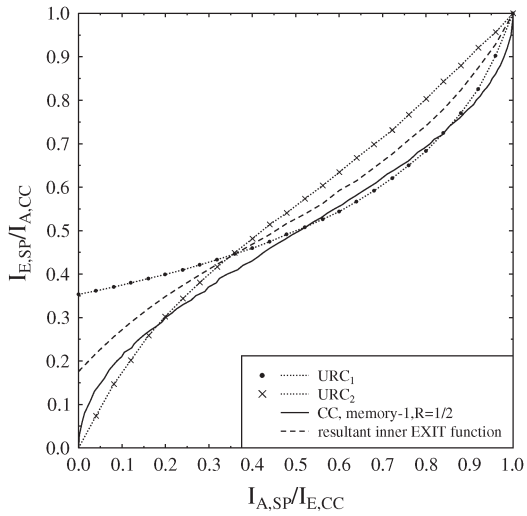

Fig. 3. Comparison of the convergence behavior of the precoded systems using the STBC-SP-BICM demapper employing an IrURC precoder, i.e., URC_1 and URC_2, as detailed in Section V. The EXIT charts shown are based on the parameters outlined in Table II when operating at $E_b/N_0 = 2$ dB.

rate (BER) at a reduced overall complexity. An exhaustive computer search is carried out for URC generator polynomials having memories of 1, 2, and 3. We plotted all the possible EXIT curves of all of these URCs, and the two specific URCs were selected for System 5 employing a Gray mapping, which had very differently shaped EXIT curves, because they allowed the combined URC-SP module to have as flexible an EXIT-curve shape as possible. This facilitated the creation of a marginally open EXIT tunnel and, hence, near-capacity operation. Then, we replaced the URC by the proposed IrURC.

These two different URCs had memories of 1 and 3, respectively, and their generator polynomials were defined in the form of (G_1, G_2), where G_1 and G_2 denote the feedforward and feedback polynomials in octal format. We refer to these URCs as URC_1 and URC_2, which are represented by $(2_8, 3_8)$ and $(16_8, 17_8)$, respectively.

The EXIT chart-matching algorithm in [16] can be used to create a near-capacity irregular scheme, where a certain fraction of the bits is encoded by one of the constituent URCs. By exploiting that the open area of the EXIT tunnel is characteristic of how close the system operates to the capacity, we can adjust the weighting coefficient β of each URC subcode to create a marginally open EXIT tunnel, which guarantees convergence to the (1, 1) point.

VI. Results and Discussion

In this section, we employ a 1/2-rate outer CC, whereas the rest of the parameters are summarized in Table II. A total of 5000 frames containing 2560 CC-encoded bits were transmitted for the sake of our BER evaluations. The effective system throughput of our SP-16 system is $(2 \text{ b/channel use}) \times 1/2 = 1$ b/channel use, whereas that of our SP-256 system becomes $(4 \text{ b/channel use}) \times 1/2 = 2$ b/channel use.

We focus our attention on two main schemes: First, the precoded scheme based on SP-16 constellations is considered, which invokes a URC precoder for improving the iterative convergence performance. Second, the SP-256 STBC-SP-BICM scheme dispensing with the URC precoder is used for comparison with the classic 4-b/symbol 16QAM scheme. Note from Fig. 2 that the EXIT characteristic of the precoded-SP mapper reaches the point of perfect convergence at (1, 1). However, at $E_b/N_0 = 4$ dB, the EXIT characteristic of both the precoded L1-BSA and L2-BSA schemes of Table I dips below the outer CC's EXIT curve; thus, the iterations are curtailed at $E_b/N_0 = 6$ dB. Nonetheless, beyond $E_b/N_0 = 6$ dB, the precoded-SP EXIT curves create an open EXIT tunnel, allowing the iterative decoding trajectory to reach the point of perfect convergence. We also observe that the precoded-Gray SP mapper in Table I exhibits the highest $I_{E,SP}$ starting point in Fig. 2 and allows a faster convergence by providing a wider EXIT tunnel. This demonstrates that the precoded-Gray mapping potentially results in an improved performance gain for our STBC-SP-BICM scheme.

Based on the EXIT chart analysis in Fig. 2, to achieve an infinitesimally low BER with the advent of a relatively long interleaver, we do not require a strong outer memory-4 CC. Fig. 2 also characterizes the memory-1 1/2-rate CC, which exhibits a more diagonally oriented EXIT curve shape with a lower I_E starting point. Note that we can achieve convergence to the (1, 1) point at a much lower SNR when employing precoded Gray mapping. We further enhance the system with a flexible IrURC substituting the memory-1 URC component. We invoke the IrURC to obtain an open EXIT tunnel at a low E_b/N_0 value.

Fig. 3 shows the EXIT characteristics of both URC_1 and URC_2. Observe that none of the EXIT functions guarantees an open EXIT tunnel. However, with the aid of the IrURC, we can create an open EXIT tunnel when using the weighting coefficient β_i for URC_i. Here, we invoke $\{\beta_1, \beta_2\} = \{0.5, 0.5\}$. This corresponds to encoding half of bit stream $\mathbf{v}$ in Fig. 1 by URC_1 and URC_2, respectively. The resultant inner EXIT function shown as a dotted line in Fig. 3 now provides an open tunnel for iterative convergence to the (1, 1) point.

Our identical-throughput benchmarker is based on a STBC-QPSK-BICM structure, which is constituted by the direct serial concatenation of STBC and CC with conventional QPSK modulation, where the outer CC maps the output symbols to a 2-D QPSK UP-based modulator. The CC coding rate for this STBC-QPSK-BICM benchmarker is also 1/2, giving an effective system throughput of 2 b/channel use $\times\, 1/2 =$ 1 b/channel use. Fig. 4 compares the BER performance of the precoded Gray mapping to that of the sphere-packing constellation point set mapping scheme for the STBC-SP-BICM system. The precoded Gray scheme's BER curve dips further below 10^{-5} at $E_b/N_0 = 4$ dB than that of the sphere-packing constellation point set mapping, which exhibits an error floor. Our other benchmarker constituted by a conventional BI-STCM-ID scheme employing QPSK and UP reaches BER $= 10^{-5}$ at $E_b/N_0 = 6.5$ dB after nine iterations. It is worth noting that the introduction of the URC precoder imposes only moderate

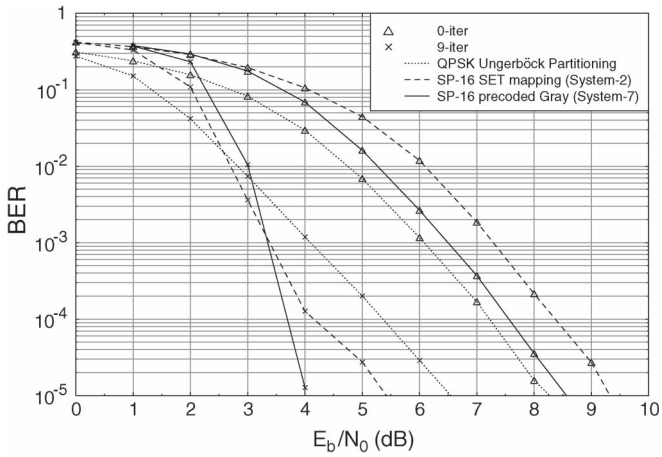

Fig. 4. Performance comparison of the BER performance for our STBC-SP-BICM system employing SP in conjunction with $M = 16$ invoking sphere-packing constellation point set mapping and a precoded Gray SP demapper. A benchmarker of BI-STCM-ID employing Ungerböck's partitioning is shown with conventional QPSK modulation.

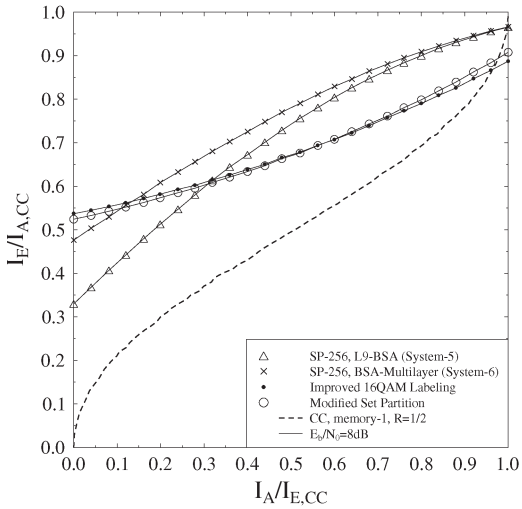

Fig. 5. EXIT chart of an STBC-SP-BICM scheme employing $M = 256$ SP demapper with different mapping strategies. A comparison is made with MSP mapping [6] and improved 16QAM labeling [8] when operating at an $E_b/N_0 = 8$ dB.

complexity increase since it employs a simple URC encoder while achieving significant BER improvement.

The EXIT chart in Fig. 5 is plotted to demonstrate the attainable performance improvement of our STBC-SP-BICM scheme employing our novel SP-256 arrangement, which uses $M = 256$ SP signal constellation points, as detailed in Section IV. A comparison with the modified set partitioning (MSP) scheme in [6] and with the improved 16QAM labeling of [8] used in the context of the existing BI-STCM-ID system [9] is also beneficial. The EXIT characteristics of the L9-BSA and BSA-multilayer mapping schemes outlined in Section IV are shown in Fig. 5. We employ a 1/2-rate CC for both the classic 16QAM and SP-256 schemes, which have an effective throughput of $4\ \text{b}/(\text{channel use}) \times 1/2 = 2\ \text{b}/(\text{channel use})$.

Observe in Fig. 5 that, at $E_b/N_0 = 8$ dB, the SP-256 scheme using the L9-BSA mapper emerges from a lower $I_{E,SP}$ value, but it reaches a higher point of convergence compared to both the MSP and the improved 16QAM labeling detailed in [6] and [8]. By mapping the bits to SP constellation points across different SP layers, the BSA-multilayer mapper becomes capable of commencing from a higher EXIT chart starting point, compared to the single-layer L9-BSA mapper. This also demonstrates that our proposed BSA-multilayer scheme becomes capable of outperforming the other mappers, provided that a sufficiently high number of iterations are affordable. The EXIT function of the memory-1 CC is shown in Fig. 5, demonstrating that our System 5 and System 6 are capable of achieving iterative convergence as a benefit of having an open EXIT tunnel. The 2-D 16QAM using the improved labeling, however, fails to provide an open tunnel, although its crossover point is beyond $I_A \approx 0.95$, which is indicative of a good BER performance. This is particularly beneficial when we are able to use a low-complexity outer CC of memory 1, which has only two-trellis decoding states.

VII. Conclusion

Novel STBC-SP-BICM schemes that are capable of exploiting both the spatial diversity of STBC and the joint-space-time symbol design of two time slots have been proposed. The proposed schemes benefit from a substantial diversity gain with the advent of different mapping strategies for $M = 16$. Precoded mapping was designed for our STBC-SP-BICM system, with the objective of exploiting the resultant recursive nature of our SP demapper for the sake of approaching the point of perfect convergence at (1, 1). An irregular structure of IrURC has been introduced to obtain a flexible open EXIT funnel for effective iterative convergence. We further extended our design to an SP scheme using $M = 256$ and two different mappers. We compared our scheme's convergence behavior with that of the identical-throughput MSP [6] and with the improved 16QAM labeling in [8], with the aid of EXIT chart analysis. The results show the presence of a wider EXIT tunnel, leading to an increased iteration gain for our new scheme.

References

[1] S. M. Alamouti, "A simple transmitter diversity scheme for wireless communications," *IEEE J. Sel. Areas Commun.*, vol. 16, no. 8, pp. 1451–1458, Oct. 1998.

[2] V. Tarokh, H. Jafarkhani, and A. R. Calderbank, "Space-time block codes from orthogonal designs," *IEEE Trans. Inf. Theory*, vol. 45, no. 5, pp. 1456–1467, Jul. 1999.

[3] O. R. Alamri, B. L. Yeap, and L. Hanzo, "A turbo detection and sphere-packing-modulation-aided space-time coding scheme," *IEEE Trans. Veh. Technol.*, vol. 56, no. 2, pp. 575–582, Mar. 2007.

[4] E. Zehavi, "8-PSK trellis codes for a Rayleigh channel," *IEEE Trans. Commun.*, vol. 40, no. 5, pp. 873–883, May 1992.

[5] X. Li and J. A. Ritcey, "Bit-interleaved coded modulation with iterative decoding," *IEEE Commun. Lett.*, vol. 1, no. 6, pp. 169–171, Nov. 1997.

[6] A. Chindapol and J. A. Ritcey, "Design, analysis, and performance evaluation for BICM-ID with square QAM constellations in Rayleigh fading channels," *IEEE J. Sel. Areas Commun.*, vol. 19, no. 5, pp. 944–957, May 2001.

[7] F. Schreckenbach, N. Görtz, J. Hagenauer, and G. Bauch, "Optimization of symbol mappings for bit-interleaved coded modulation with iterative decoding," *IEEE Commun. Lett.*, vol. 7, no. 12, pp. 593–595, Dec. 2003.

[8] Y. Huang and J. A. Ritcey, "Improved 16-QAM constellation labeling for BI-STCM-ID with the Alamouti scheme," *IEEE Commun. Lett.*, vol. 9, no. 2, pp. 157–159, Feb. 2005.

[9] Y. Huang and J. A. Ritcey, "Tight BER bounds for iteratively decoded bit-interleaved space-time coded modulation," *IEEE Commun. Lett.*, vol. 8, no. 3, pp. 153–155, Mar. 2004.

[10] A. S. Mohammed, W. Hidayat, and M. Bossert, "Multidimensional 16-QAM constellation labeling of BI-STCM-ID with the Alamouti scheme," in *Proc. IEEE WCNC*, Apr. 2006, vol. 3, pp. 1217–1220.

[11] A. Paulraj, R. Nabar, and D. Gore, *Introduction to Space-Time Wireless Communications*. Cambridge, U.K.: Cambridge Univ. Press, May 2003.

[12] W. Su, Z. Safar, and K. J. R. Liu, "Space-time signal design for time-correlated Rayleigh fading channels," in *Proc. IEEE Int. Conf. Commun.*, Anchorage, AK, May 2003, pp. 3175–3179.

[13] D. Divsalar, S. Dolinar, and F. Pollara, "Serial concatenated trellis coded modulation with rate-1 inner code," in *Proc. IEEE Global Telecommun. Conf.*, Nov. 2000, pp. 777–782.

[14] J. H. Conway and N. J. Sloane, *Sphere Packings, Lattices and Groups*. Berlin, Germany: Springer-Verlag, 1999.
[15] S. T. Brink, "Convergence behavior of iteratively decoded parallel concatenated codes," *IEEE Trans. Commun.*, vol. 49, no. 10, pp. 1727–1737, Oct. 2001.
[16] M. Tüchler, "Design of serially concatenated systems depending on the block length," *IEEE Trans. Commun.*, vol. 52, no. 2, pp. 209–218, Feb. 2004.

Maximum-Likelihood Sequence Detection in Time- and Frequency-Selective MIMO Channels With Unknown Order

Manuel A. Vázquez and Joaquín Míguez, *Member, IEEE*

***Abstract*—In the equalization of frequency-selective multiple-input–multiple-output (MIMO) channels, it is usually assumed that the length of the channel impulse response (CIR), which is also referred to as the channel order, is known. However, this is not true in most practical situations, and it is a common approach to overestimate the channel order to avoid the serious performance degradation that occurs when the CIR length is underestimated. Unfortunately, the computational complexity of maximum-likelihood sequence detection (MLSD) in frequency-selective channels exponentially grows with the channel order; hence, overestimation can actually be undesirable because it leads to more expensive and inefficient receivers. In this paper, we introduce an algorithm for MLSD that incorporates the full estimation of the MIMO CIR parameters, including its order. The proposed technique is based on the *per-survivor processing* (PSP) methodology; it admits both blind and semiblind implementations, depending on the availability of pilot data, and is designed to work with time-selective channels. In addition to the analytical derivation of the algorithm, we provide computer simulation results that illustrate the effectiveness of the resulting receiver.**

***Index Terms*—Channel order estimation, joint channel and data estimation, multiple-input–multiple-output (MIMO), per-survivor processing (PSP).**

I. Introduction

Maximum-likelihood sequence detection (MLSD) in multiple-input–multiple-output (MIMO) channels is a computationally hard task. The complexity of conventional MLSD receivers exponentially grows with the number of input streams for the case of flat-fading channels [1]. If the channel is frequency selective, then the received signal suffers from intersymbol interference (ISI), and the detector complexity also exponentially grows with the length of the symbol-rate channel impulse response (CIR) [2]. We hereafter refer to this length as the *channel order*.

Manuscript received November 23, 2007; revised March 17, 2008 and March 31, 2008. First published May 7, 2008; current version published January 16, 2009. This work was supported in part by the Ministry of Education and Science of Spain under Grant TEC2007-68020-C04-01 and Grant TEC2006-13514-C02-01/TCM, by *Xunta de Galicia* under Grant PGIDIT06TIC10501PR, and by the local government of Madrid under Project PRO-MULTIDIS-CM (S0505/TIC/0223). The review of this paper was coordinated by Prof. X.-G. Xia.

M. A. Vázquez is with the Departamento de Electrónica y Sistemas, Universidad da Coruña, 15071 A Coruña, Spain (e-mail: mvazquez@udc.es).

J. Míguez is with the Departamento de Teoría de la Señal y Comunicaciones, Universidad Carlos III de Madrid, 28911 Leganés, Madrid, Spain (e-mail: joaquin.miguez@uc3m.es).

Color versions of one or more of the figures in this paper are available online at http://ieeexplore.ieee.org.

Digital Object Identifier 10.1109/TVT.2008.924996

When perfect channel state information is available at the receiver, MLSD is carried out by means of the Viterbi algorithm (VA) [2]. When the CIR is not known, per-survivor processing (PSP) techniques [3], [4] have been suggested as a means to jointly handle sequence detection and channel estimation. The term PSP refers to a family of trellis search methods that extended the VA by combining data detection and channel estimation. The key idea is to maintain a set of *survivor* paths (i.e., sequences of symbols) arriving at each trellis node instead of a single path, as in the conventional VA. For each survivor path, a CIR estimate is computed, and a likelihood is assigned, conditional on the symbols and the resulting channel estimate. Detection reduces to selecting the most likely survivor, which, therefore, yields a sequence of symbols and an explicit CIR estimate.

However, CIR estimation is almost invariably carried out based on an assumed length, which is selected prior to the detection/estimation process. Since accurate channel-order estimation can be hard, and it is known that underestimation severely degrades receiver performance, it is common practice to overestimate the order [5]. Unfortunately, the choice of a CIR length larger than actually needed implies an exponential increase in computational complexity, more uncertainty in the channel estimation procedure (since more parameters need to be estimated) and, consequently, performance degradation.

Information-theoretical methods, such as the minimum description length (MDL) [6] or the Akaike information criteria [7], have been proposed for channel order estimation, but such techniques tend to overestimate for high signal-to-noise ratios (SNRs) [8], [9]. In [10], a novel approach for the model order selection problem is proposed based on the theory of sufficient statistics, and superior reliability compared with MDL is claimed. This method, which is known as the conditional model order estimation (CME), has been applied to MIMO communication channels in [11]. However, CME is based on the assumption that the CIR is fixed for the duration of a complete data frame, and the processing of the block of available observations is performed offline, in batch mode. A different approximation to the problem can be found in [12], where a method for the estimation of the *effective channel order* is introduced based on the minimization of a combination of cost functions. However, this technique is designed for single-input–multiple-output channels, as well as under the assumption that the channel is fixed during the transmission of a symbol frame. Finally, particle filtering methods have also been proposed for the equalization of frequency-selective channels with unknown order [13]. Although such algorithms are effective, their complexity can be prohibitive, even for the single-input–single-output case shown in [13]. A similar technique for orthogonal frequency-division multiplexing (OFDM) MIMO systems is presented in [14].

In this paper, we introduce a method based on the PSP principle for the equalization of frequency- and time-selective MIMO channels with unknown order. Compared to conventional PSP receivers, the key features of the new technique are as follows: 1) the computation of a maximum *a posteriori* (MAP) estimate of the channel order for each survivor path and 2) the selection of survivors, which is globally performed instead of per arrival state. Compared with existing channel order estimation methods, the proposed algorithm enables optimal *a posteriori* estimation of the channel order and the resulting CIR, conditional on the received signals and the symbols in the survivor path, and is specifically designed for time-selective environments. Suboptimal versions of the method are also discussed and numerically assessed.

The remainder of this paper is organized as follows: In Section II, the discrete-time signal model of a MIMO transmission system with frequency- and time-selective channels is described. The proposed algorithms are introduced in Section III. Computer simulation results